Salt-Induced Association of β-Lactoglobulin by Light and X-ray Scattering

Giancarlo Baldini,[†] Sabrina Beretta,[†] Giuseppe Chirico,[†] Hermann Franz,[‡] Elisabetta Maccioni,[§] Paolo Mariani,*[,§] and Francesco Spinozzi[§]

Dipartimento di Fisica and Istituto Nazionale per la Fisica della Materia, Università di Milano, Via Celoria 16, I-20133 Milano, Italy; Hamburger Synchrotronstrahlungs Labor am DESY, Notkestrasse 85, 22603 Hamburg, Germany; and Istituto di Scienze Fisiche and Istituto Nazionale per la Fisica della Materia, Università di Ancona, Via Ranieri 65, I-60131 Ancona, Italy

Received May 4, 1999; Revised Manuscript Received July 9, 1999

ABSTRACT: β-Lactoglobulin, a protein belonging to the lipocaline family, is studied by Photon correlation spectroscopy and small angle X-ray scattering in acidic solutions (pH = 2.3) and at ionic strengths in the range 7−507 mM. Both experiments give a clear evidence of a protein monomer−dimer equilibrium affected by the ionic strength of the solution. The interparticle interactions are determined by means of Photon correlation spectroscopy by following the trend of the protein diffusion coefficient versus concentration (from 0.2 to 25 g/L) at ionic strengths of 7 and 107 mM. From a detailed analysis, estimates of the protein charge, hydrodynamic radius, and dimeritazion fraction have been obtained. Small angle X-ray scattering measurements performed versus ionic strength (from 7 to 507 mM) in dilute solutions (10 g/L) allow an independent estimate of the dimerization fraction. A global fit of the SAXS scattered intensities at different salt concentrations using a simple electrostatic model for the aggregation mechanism is presented. As a result, the dissociation free energy has been obtained as a function of the ionic strength, yielding an excellent agreement with photon correlation spectroscopy data.

1. Introduction

β-Lactoglobulin (β-LG) is a 18 400 Da protein that belongs to the lipocaline family and is abundantly contained in mammalian milk. This protein has 162 residues with eight β-anti-parallel sheets and one α-helix chain. The quaternary structure of β-LG protein has been investigated by several techniques, like sedimentation equilibrium,[1] infrared spectroscopy,[2,3] fluorescence,[4,5] X-ray,[6,7] and light scattering.[8,9] At neutral pH, the structure is dimeric, while at acidic pH (a condition more similar to the physiological one) the quaternary structure is lost, with a partial dissociation into two monomers still showing a fairly ordered structure.[10−13] A dependence of the monomer−dimer equilibrium (and of the folding processes) on the ionic strength has been reported.[4,8,14,15]

The β-LG function is still not fully clarified: it is believed that the function is connected to transport processes inside the cell, due to the ability of this protein to bind small ligands (ellipticin, some fatty acids, sodium dodecyl sulfate, and retinol).[16] In particular, each monomer has an internal hydrophobic site, formed by the characteristic β-barrel, and one (or more) less characterized site on the surface. It should be noticed that the role of the quaternary structure in the binding processes should be relevant since, for example, β-LG binds one retinol molecule per monomer, whereas ellipticin binds in a ratio of one molecule per dimer.[17]

The study of the β-LG aggregation properties in solution, and especially under acidic conditions, can therefore be a valuable piece of information in understanding some aspects of its function.[18] However, only few studies on the association behavior of β-LG and on its dependence on the ionic strength have been reported,[4,8,14] and though the measurements were performed down to an ionic strength of 13 mM,[8] the dissociation constant was not determined at the lowest salt contents because electrostatic interactions dominate. Moreover, also the knowledge of the effective protein charge under different conditions may help in formulating a more comprehensive description of the different contributions (e.g. polar versus hydrophobic) to the protein−protein and protein−ligand interactions.[19] However, it is a delicate matter to separate these contributions, because of the variety of subtle effects related to the polyionic character of the protein.[20] This has limited the quantitative analysis of the previous studies to relatively high ionic strength (≥30 mM).

Structural changes, such as those involved in a dimerization process, influence the average protein size and can be monitored by several techniques. Among them, radiation scattering is one of the most suitable approaches,[21−26] due to its small perturbing effects on the system. In particular, conformational changes can be tracked by measuring the diffusion properties of the protein by light scattering (the typical length scale is 100−1000 Å). From the analysis of the relaxation rate of the autocorrelation function of the scattered light, information on the mutual diffusion coefficient of the polymer can be obtained, and while studying the average light scattering rate as a function of the protein concentration, the first virial coefficient can be derived. Furthermore, information about the molecular size of the protein can be obtained in terms of hydrodynamic radiius extrapolating to low concentration the diffusion coefficients. Finally, the trend of the diffusion

* Author for correspondence. Istituto di Scienze Fisiche, Facoltà di Medicina, Università di Ancona, Via Ranieri 65, I-60131 Ancona, Italy. Phone: 39.071.2204608. Fax: 39.071.2204605. E-mail: mariani@popcsi.unian.it.
[†] Università di Milano.
[‡] Hamburger Synchrotronstrahlungs Labor am DESY.
[§] Università di Ancona.

10.1021/ma990709u CCC: $18.00
Published on Web 08/28/1999

coefficient versus the concentration can give additional information on protein−protein interactions.

Due to the relatively small size of the particle, small angle X-ray scattering from a protein solution can give valuable information on the aggregation state and on the average low-resolution shape of the protein.[24,27] As a matter of fact, the wavelength of this radiation matches the typical protein size.

In this work, photon correlation spectroscopy (PCS) and small angle X-ray scattering (SAXS) have been used to analyze the association behavior of β-lactoglobulin under acidic conditions and to study the dependence of the aggregation process to the ionic strengths of the solution. The aim and the novelty of the present work are to give a quantitative analysis *at different length scales* of the dimerization process of β-LG at pH = 2.3 and its modulation by the ionic strength in a range of NaCl concentration (0−500 mM) that extends previous studies. This is achieved by following the average and the fluctuations of the scattered light versus the protein concentration and the change in the form factor measured by small-angle X-ray scattering versus the solution ionic strength. While the light scattering measurements yield information on the interparticle interactions and on the extent of protein aggregation, the X-ray scattering measurements, combined with a structural model for the β-LG monomer and dimer, give an estimate of the dissociation process. As a result, a detailed analysis of the modulation of the protein−protein and protein−electrolyte interactions by the ionic strength is obtained. Introducing a simple polyelectrolyte model for protein[28] allows a quantitative estimate of the electrostatic and nonelectrostatic contributions to the dissociation free energy of β-LG at acidic pH values for a wide range of ionic strengths. Since the effects of the interparticle interactions on the measurements here presented are negligible, the comparison of the outputs from the two scattering techniques is a sensitive check on the correct interpretation of the experimental results.

2. Theoretical Background

In the following we refer explicitly to a protein solution which contains monomers (m) and dimers (d) in mutual equilibrium according to

$$K_{dis} = \exp(-\Delta G_{dis}/k_B T) \tag{1}$$

where ΔG_{dis} is the molecular dissociation free energy. K_{dis} is the dissociation constant related to the molar concentration of monomers, [m], and dimers, [d], by $K_{dis} = [m]^2/[d]$. The dissociation constant can be also written in terms of the weight protein concentration, C,

$$K_{dis} = \frac{2C\alpha^2}{(1-\alpha)M_m} \tag{2}$$

where M_m is the molecular weight of the protein in the monomeric form and α is the monomer fraction. Being that C_m and C_d are the weight concentrations of the protein in the monomeric and dimeric forms (i.e. $C = C_m + C_d$), the α fraction is defined by

$$\alpha = \frac{C_m}{C_m + C_d} \tag{3}$$

If the protein in solution is charged (polyion), the dissociation free energy, ΔG_{dis}, in eq 1 can be written in term of two contributions,

$$\Delta G_{dis} = \Delta G_{el} + \Delta G_{nel} \tag{4}$$

in which ΔG_{el} is the electrostatic term and ΔG_{nel} is a term referring to nonelectrostatic and entropic contributions. In a simple approximation, for a monomer−dimer equilibrium, ΔG_{el} can be calculated using a Debye−Hückel model in which both monomer and dimer are assumed to be spheres of constant charge density.[28] It results that

$$\Delta G_{el} = 2G_{el}(m) - G_{el}(d) \tag{5}$$

$$G_{el}(j) = \frac{q^2 Z_j^2}{2\epsilon R_j}\left[1 - \frac{\kappa_D R_j}{1 + \kappa_D(R_j + a)}\right] \tag{6}$$

where Z_j and R_j are the number of *effective* charges and the radius of the jth species, respectively, a is the radius of the counterions, ϵ is the solvent dielectric constant, and q is the proton charge. κ_D is the Debye screening factor based on all added electrolytes and on counterions,[29]

$$\kappa_D = \left[\frac{8\pi N_A q^2}{1000\epsilon k_B T}\left(I_S + \left|Z_j\right|\frac{C}{2M_j}\right)\right]^{1/2} \tag{7}$$

where N_A is the Avogadro number and $I_S = (1/2)\sum_i c_i z_i^2$ is the ionic strength due to all added electrolyte species i of molar concentration c_i and charge z_i in solution.

2.1. Light Scattering. The excess scattering intensity for a single-component colloid in an isotropic solution depends on the protein concentration, C, and on the modulus of the scattering vector, **Q**. At low concentrations, one can write

$$I(Q) = \kappa_{LS} P(Q) S(Q) MC + B_{LS} \simeq \kappa_{LS} P(Q) MC\,(1 + K_S C) + B_{LS} \tag{8}$$

where M is the particle molecular weight, K_S is the intensity interaction constant, and κ_{LS} and B_{LS} are experimental parameters depending on the optic setup and the scattering power of the solvent. The averaged form factor, $P(Q)$, over all possible molecular orientations defines the angular dependence of the scattered radiation and, depending on the wavelength of the used radiation, may contain information on the molecular shape. The structure factor, $S(Q)$, arises from correlations in the mutual positions of nearby proteins and depends on the strength and the range of the interparticle interactions.

In the case of light scattering from proteins, the particle size (typically a few tens of angstroms) is much smaller than the inverse of the typical wave vector ($Q^{-1} \simeq 1000$ Å) and the Q-dependence of the scattered intensity is negligible, i.e. $P(Q) \simeq 1$. Moreover, the structure factor $S(Q)$ can be computed for $Q \simeq 0$ and expanded versus concentration as $(1 + K_S C)$. The scattering vector of the first peak of the structure factor $S(Q)$ is proportional to the inverse of the average protein−protein distance, and at $C \simeq 0.1$ g/L, the minimum concentration investigated here, one expects to find[30] a peak at ≃0.014 Å^{-1}, which is much larger than the typical light scattering vector (≃0.002 Å^{-1}).

In a two-component system, like a solution of monomers (m) and dimers (d), eq 8 has to be changed to

$$I(Q) \propto [\sum_{k=\mathrm{m,d}} M_k C_k (1 + \sum_{j=\mathrm{m,d}} K_{\mathrm{S},j,k} C_j)] \qquad (9)$$

where M_k and C_k are the molecular weight and the concentration of the particle of the kth species and the intensity interaction constant $K_{\mathrm{S},j,k}$ between the particles of the jth and kth species can be defined in terms of the protein−protein radial distribution function $g_{j,k}(\sigma)$ as[31]

$$K_{\mathrm{S},j,k} = -8\bar{v} + \bar{v}\int_{x_c}^{\infty} 24(1+\sigma)^2 (g_{j,k}(\sigma) - 1)\, \mathrm{d}\sigma \qquad (10)$$

In this equation, $\bar{v}$ is the protein specific volume, σ is the normalized interparticle distance ($\sigma = (r - R_j - R_k)/(R_j + R_k)$, where R_j and R_k are the radii of the particles of the jth and kth species and r is their distance), and $x_c = 0.06$ is due to the width of the hydration/Stern layer.[32] The use of this integration cutoff can also be related to short range interactions due, for example, to hydrophobic terms and possibly hydrogen bonding, involving an atomic description of the protein−protein interaction which is beyond the aim of the present approximate treatment. Here, as in similar studies on the protein aggregates and their interaction energy,[23,32] an implicit assumption of spherical symmetry has been made, the validity of which deserves further detailed investigation. The radial distribution function can be written, at the lowest order in the protein concentration, as

$$g_{j,k}(\sigma) = \exp(-U_{j,k}(\sigma)/k_{\mathrm{B}}T) \qquad (11)$$

At low salt concentrations,[32] the interaction potential $U_{j,k}(\sigma)$ is given by the so-called DLVO[33] model, which is the sum of a screened repulsive Coulomb potential[34]

$$U^{\mathrm{C}}_{j,k}(\sigma) = \frac{q^2 Z_i Z_k \exp[-\kappa_{\mathrm{D}}(R_j + R_k)\sigma]}{\epsilon(R_j + R_k)(1 + \kappa_{\mathrm{D}} R_j)(1 + \kappa_{\mathrm{D}} R_k)(1 + \sigma)} \qquad (12)$$

and a van der Waals attractive potential

$$U^{H_{\mathrm{A}}}_{j,k}(\sigma) = -\frac{H_{\mathrm{A}}}{12}\left\{\frac{1}{(1+\sigma)^2} + \frac{1}{(\sigma+\sigma^2)} + 2\ln\left[\frac{2\sigma+\sigma^2}{(1+\sigma)^2}\right]\right\} \qquad (13)$$

where H_{A} is the Hamaker constant. A general agreement on the value of H_{A} is not available. However, although reported values of H_{A} span over a wide range, $0.5k_{\mathrm{B}}T \le H_{\mathrm{A}} \le 10k_{\mathrm{B}}T$, recent works on small globular proteins[32,35] suggest values closer to the upper limit.

Useful additional information can be also obtained by looking at the temporal fluctuations of the light scattered by the protein solution. The autocorrelation function of the scattered light decays exponentially to $\langle I(Q)\rangle^2$ and its relaxation rate, Γ, is related to the mutual diffusion coefficient D by

$$D = \frac{\Gamma}{Q^2} \qquad (14)$$

For a two-component system, where the molecular masses of the two species differ only by a factor 2, the autocorrelation function is still well-described by a single exponential.[22,23] In such a case, the measured mutual diffusion coefficient can be formally written as[23]

$$D = \sum_{j=\mathrm{m,d}} C_j M_j D_{j,0} (1 + \sum_{k=\mathrm{m,d}} C_k K_{\mathrm{D},j,k}) / \sum_{j=\mathrm{m,d}} C_j M_j \qquad (15)$$

where $D_{j,0}$ is the low concentration limit of the diffusion coefficient of the jth species. Analogously to the intensity interaction constant $K_{\mathrm{S},j,k}$ (eq 10), an approximate expression of the diffusion interaction constant $K_{\mathrm{D},j,k}$, which is yet to be completely established for monodisperse charged sphere systems, can be written in terms of the protein−protein radial distribution functions[36−38] as

$$K_{\mathrm{D},j,k} = 1.56\bar{v} + \bar{v}\int_{x_c}^{\infty} (g_{j,k}(\sigma) - 1)[0.706 + 11.89(1+\sigma) - 1.69/(1+\sigma) - 24(1+\sigma)^2]\, \mathrm{d}\sigma \qquad (16)$$

Therefore, the parameters involved in the computation of the interaction constants are the protein charge and radius.

2.2. Small Angle X-ray Scattering. It is well-known that small angle scattering of X-ray (or neutrons) from biological macromolecules in solution yields information on their overall shape and dimension. Because of the dependence on the particle structure, scattering data can be extremely sensitive to structural and conformational changes, as well as to molecular associations in solution. The scattering from proteins in a diluted solution (in order to avoid ambiguity due to intermolecular association, we will refer to them also as scattering particles) can be described by the so-called two-phase model, where identical scattering centers with homogeneous electron density ρ are randomly oriented in a matrix (the solvent) with different electron density ρ_{s}.[27] In this case, the excess X-ray scattering intensity reduces to

$$I(Q) = \kappa_{\mathrm{XR}} \frac{C}{M} (\Delta\rho V)^2 P(Q) S(Q) + B_{\mathrm{XR}} \qquad (17)$$

where κ_{XR} is a calibration factor, B_{XR} is a flat background, $\Delta\rho = (\rho - \rho_{\mathrm{s}})$ is the contrast, V is the scattering particle volume, $P(Q)$ is the averaged squared form factor which depends on the size and shape of the scattering particles,[27] and $S(Q)$ is the structure factor. To estimate the effect of the structure factor on the X-ray scattering curves, which could reflect the presence of interparticle interactions, we calculated the $S(Q)$ function. As already reported in ref 14, where SANS data of β-LG at pH = 2 and low salt concentration were analyzed, we used a hard sphere model,[39] considering both monodisperse and polydisperse spheres with volumes equivalent to β-LG monomer and dimer and volume fraction corresponding to the experimental concentration of 10 g/L. The results show that interference effects can be neglected for Q larger than about 0.06 Å^{-1}, and therefore, in the investigated Q range it has been assumed that $S(Q) = 1$.

In a two-component system, like the monomer−dimer solution, the scattering intensity is a weighted sum of the single form factors $P_j(Q)$ and can be written in terms of α, the fraction of protein in the monomeric form (see eq 3):[27]

$$I(Q) = \kappa_{\mathrm{XR}} \frac{C}{M_{\mathrm{m}}} (\Delta\rho V_{\mathrm{m}})^2 [\alpha P_{\mathrm{m}}(Q) + 2(1-\alpha) P_{\mathrm{d}}(Q)] + B_{\mathrm{XR}} \qquad (18)$$

An isotropic Fourier transform connects the form factor $P_j(Q)$ to the corresponding $p_j(r)$, i.e. the probability of finding couples of small volume elements at a distance r within the entire volume of the scattering particle j,

$$P_j(Q) = \int_0^\infty p_j(r)\frac{\sin(Qr)}{Qr}\,dr \leftrightarrow p_j(r) = \frac{2r}{\pi}\int_0^\infty P_j(Q)\,Q\,\sin(Qr)\,dQ \quad (19)$$

At small Q, the form factor can be approximated by the so-called Guinier law,[27] $P_j(Q) = e^{-Q^2R_{g,j}^2/3}$, where $R_{g,j}$ is the gyration radius of the jth species, defined for an homogeneous particle by

$$R_{g,j}^2 = \frac{1}{2}\int_0^\infty r^2 p_j(r)\,dr \quad (20)$$

The Guinier approximation is strictly valid only for $QR_{g,j} \simeq 1$.[27]

For a two-component system, the scattering intensity can be then approximated by

$$I(Q) = I(0)e^{-Q^2R_{g,a}^2/3} \quad (21)$$

where, according to the eq 18 (with $B_{XR} = 0$),

$$I(0) = \kappa_{XR}\frac{C}{M_m}(\Delta\rho V_m)^2(2-\alpha) \quad (22)$$

and $R_{g,a}$ represents an apparent radius of gyration. When the radii of gyration of the two components are known, we obtain[6,27]

$$R_{g,a}^2 = \frac{\alpha R_{g,m}^2 + 2(1-\alpha)R_{g,d}^2}{2-\alpha} \quad (23)$$

Independently from any a priori structural assumption (like $R_{g,j}$ or V_j in eqs 22 and 23), useful information can be obtained from a distance distribution function $p(r)$ directly calculated from the experimental scattering function $I(Q)$. Here we calculated the $p(r)$ functions using a multipole expansion method recently improved by applying group theory and maximum entropy.[40] The application of this method to scattering data relative to particles in equilibrium between different states leads to a reconstructed particle shape that will be a weighted average of the different aggregation forms. This average shape is therefore not directly related to the real shape of any of the protein species in solution but gives a representation of their relative abundance and can be used to calculate an accurate averaged $p(r)$. It should be observed that from the $p(r)$ function, the maximum particle dimension, d_{max}, can be estimated, as the vector modulus r where the $p(r)$ becomes zero.

The Kratky plot, i.e. the $I(Q)Q^2$ vs Q plot, is another useful tool in SAXS analysis to describe the structural characteristic of a polymer molecule.[24] This plot is particularly valuable for the structural characterization of globular particles and for the detection of folded states.[41−43] For a globular protein, the Kratky plot shows a peak, the position of which depends on its gyration radius, R_g. By contrast, the Kratky plot for an unfolded protein (which behaves like a chain molecule with random-coil-like conformation) shows a monotonously increasing curve with a plateau.[42] Therefore, a peak in the Kratky plot indicates the presence of a compact globular structure: any shift on the peak position reflects changes on the R_g value (R_g is larger when the peak moves to lower Q), but variations on the peak width and steepness indicate that there are also significant differences on the protein (secondary) structure.

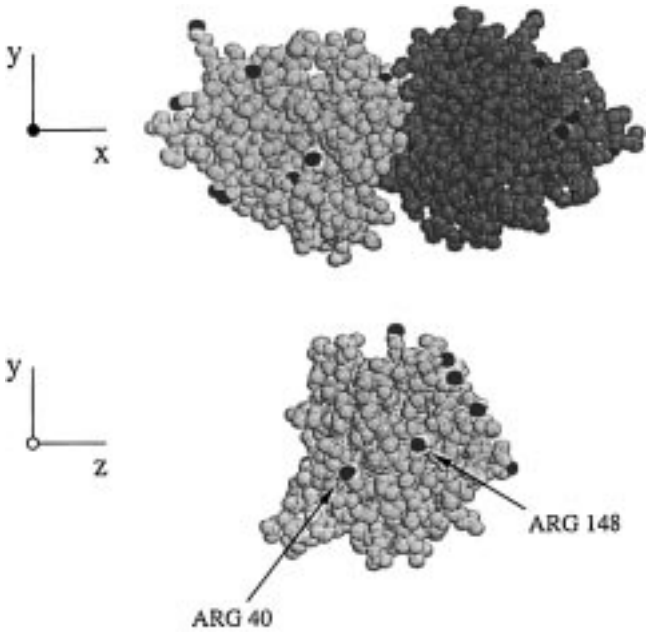

Figure 1. Three-dimensional representation of the Protein Data Bank[45] structure of dimer and monomer of β-LG. RasMol 2.6 package with *spacefill* option has been used. The groups which are expected to be charged at pH = 2.3 are shown in black. The monomer has been rotated of 90° around the *y*-axis to show the monomer−monomer interface. Note that two arginines (40 and 148) are located at this interface.

3. Materials and Methods

Bovine milk β-lactoglobulin B was purified by M. Galliano and H. Monaco (University of Pavia, Italy). Protein concentration was determined spectrophotometrically by using the molecular absorption coefficient $\epsilon = 17600\ M^{-1}\ cm^{-1}$ at $\lambda = 278$ nm. All samples were prefiltered twice with 0.2 μm (Nucleopore) low protein adsorption filters. A stock protein solution ($C = 40$ g/L) was obtained by exchanging β-LG samples against a proper phosphate buffer, 12 mM H_3PO_4/0.8 mM NaOH (ionic strength $I_S = 7$ mM and pH = 2.3), by using Amicon concentration cells with 3 kDa cutoff membranes (YM3, Amicon, Beverly, MA). All used reagents were analytical grade.

3.1. Protein Model. The monomeric unit of β-LG is composed by 162 amino acid residues and has a $M_m = 18\,400$ Da; 20 amino acids are basic, so that at pH = 2.3 the monomer is expected to bear about 20 proton charges. The protein volume (excluding the solvent) has been derived from the amino acid composition and the corresponding amino acid volumes, as reported by Jacrot and Zaccai.[25,44] The volume of the monomer is $V_m = 23400$ Å^3. The crystallographic structure of β-LG both in monomeric and in dimeric form can be found in the Protein Data Bank.[45] A representation of the structure of β-LG is sketched in Figure 1. It can be observed that all the 20 basic amino acids are on the protein surface but two of them are at the monomer−monomer interface; therefore at pH = 2.3 the ratio Z_d/Z_m between the charges in the dimer and monomer could be about 1.8.

From the crystallographic structure, the distance distribution functions $p_j(r)$ of the monomer and dimer have been calculated using a Monte Carlo method similar to that described by Mariani et al.[46] In particular, the particle shape is described by a function, $s_j(\mathbf{r})$, which gives the probability that the point $\mathbf{r} \equiv (r,\omega_r)$ (where ω_r indicates the polar angles α_r and β_r) lies within the jth species. For a compact particle, the $s_j(\mathbf{r})$ function can be written in terms of a unique two-

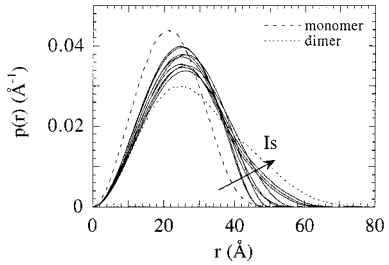

Figure 2. Distance distribution function, $p(r)$, plots of β-LG. Dashed and dotted lines are the $p(r)$ functions calculated from the monomer and dimer crystallographic coordinates, as described in the text. Continuous lines are the $p(r)$ functions obtained from the present experimental SAXS curves: following the direction indicated by the arrow, the ionic strength increases from 7 to 507 mM. For details on calculation, see sections 2.2 and 3.1.

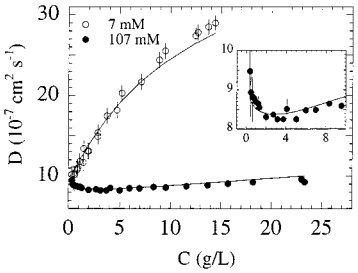

Figure 3. Mutual diffusion coefficient D of β-LG at pH = 2.3 versus protein concentration C at I_S = 7 mM (open circles) and I_S = 107 mM (filled circles). The solid lines are best fits of the data using the monomer−dimer model described in section 4.1. The inset shows the initial decrease of D at I_S = 107 mM when the concentration increases.

dimensional angular shape function, $F_j(\omega_r)$, as

$$s_j(\mathbf{r}) = \begin{cases} 1 & 0 \le r \le F_j(\omega_r) \\ \exp\{-[r - F_j(\omega_r)]^2/2\sigma_h^2\} & r > F_j(\omega_r) \end{cases} \quad (24)$$

where σ_h is the width of a Gaussian that describes the form of the border of the particle. This description takes into account the effect of the protein hydration shell, whose density can differ noticeably from that of the bulk solvent within a few angstroms distance.[47] The shape functions $F_j(\omega_r)$ are defined by the monomer and dimer envelope surfaces evaluated from the crystallographic coordinates. N random points are generated according to the probability in eq 24 and the $p_j(r)$ histograms calculated by taking into account the distances between all possible pairs of N points. The $p_j(r)$ functions obtained introducing a reasonable value σ_h = 2 Å and using N = 2000 are reported in Figure 2. The corresponding β-LG monomer and dimer radii of gyration calculated using eq 20 are $R_{g,m}$ = 16.4 Å and $R_{g,d}$ = 23.0 Å, respectively.

3.2. Light Scattering Sample. Light scattering measurements were performed at two different ionic strengths. Two concentrated protein solutions (C = 40 g/L) were prepared by exchanging the stock protein solution against the I_S = 7 mM phosphate buffer and against a I_S = 107 mM solution obtained by adding NaCl to the phosphate buffer. For PCS measurements, the solutions were diluted with the appropriate salt/phosphate solutions to the required protein concentration. Particular care has been given to the filtering procedure. The sealed PCS sample cells were rinsed carefully (400 mL) with prefiltered (0.22 μm) water by using a peristaltic pump. The samples were filtered gently through 0.1 μm Nucleopore polycarbonate filters after a few prefiltrations with higher pore size (0.2 μm Nucleopore). The final concentration and pH of each sample were determined after light scattering measurements.

3.3. SAXS Samples. Protein solutions at different ionic strengths were obtained by ionic exchange of the stock protein solution against solutions obtained by adding appropriate amounts of NaCl to the phosphate buffer. The final protein concentrations were about 10 g/L. The ionic strengths of the investigated protein solutions were 7, 17, 27, 47, 67, 87, 107, 207, and 507 mM. Reference SAXS curves for each investigated sample (see below) were taken on the corresponding solvents.

3.4. PCS Experimental Set-Up. PCS measurements were performed with the 514.5 nm argon laser line (Spectra-Physics 2025) and with typical power (750 mW) in TEM00 mode. The laser beam, vertically polarized, is spatially filtered and focused at the center of a thermostated square quartz cuvette (path length = 10 mm, Hellma). Further information on this set-up can be found elsewhere.[26]

Some changes have been made on the existing apparatus. The scattered light is detected through a multimode optical fiber whose output is sent to two PMTs (Hamamatsu, H5873P-01) by dividing the signal with a 50% cube beam splitter. The two PMT outputs are discriminated against independent thresholds and sent to the input channels of a ALV5000E/FAST digital correlator. The cross-correlation of the two signals yields then the autocorrelation function of the scattered light down to 12.5 ns lag times. Further details are being published elsewhere.[48]

All measurements have been performed at a temperature of 20 ± 0.2 °C and 90° scattering angle. Checks at different scattering angles have yielded no significant variation of the diffusion coefficient and showed no appreciable angular dependence of the average intensity.

3.5. SAXS Experiments. SAXS experiments were performed at room temperature using the SAS camera of the Physik Department of the Technische Universitat Munchen (Germany). The X-ray source was a rotating-anode generator (Siemens) operating at 18 kW. A Mo target and a vertical focusing Ge monochromator, producing λ = 0.71 Å radiation, were used. Intensity patterns were recorded on a two-dimensional gas-filled detector (Siemens High-Star). The used sample-to-detector distances of 1.51 m gives the possibility of analyzing a scattering vector Q range ($Q = 4\pi \sin\theta/\lambda$, where 2θ is the scattering angle) from 0.075 to 0.3 Å^{-1}. β-LG samples were measured in quartz capillaries with a diameter of 2 mm and a thickness of 10 μm (Hilgenberg, Malsfeld, Germany). The samples were maintained at 20 °C and the camera was evacuated to about 10^{-4} mbar to reduce the background scattering. X-ray patterns were usually obtained in about 4 h with less than a 5% counting error for the smallest angles. Since the samples scatter isotropically, data were radially averaged to improve statistics. The scattering from a solvent capillary was subtracted from the data after correction for absorption and detector sensitivity.

4. Results

4.1. Light Scattering. Measurements of the scattered light autocorrelation functions and of the average scattered intensity were performed at two ionic strengths (I_S = 7 mM and I_S = 107 mM) as a function of protein concentration ($0.2 \le C \le 25$ g/L). The mutual diffusion coefficients have been obtained by fitting the autocorrelation functions to a double exponential decay. The slower of the two decays has always small amplitude (about 2%) and a relaxation rate $\Gamma_1 \simeq 0.5$ kHz, which corresponds to particle sizes on the order of the pore diameter of the filter. This decay is therefore probably due to residual "dust" or to the presence of a small amount of very large aggregates in the protein solution. The second exponential decay has a larger relaxation rate, Γ_2, which is in the typical range of 50−60 kHz observed for protein in the same experimental conditions. Therefore, the faster component was attributed to the protein. The protein mutual diffusion coefficient was then derived from the fitted Γ_2 using eq 14 and is plotted as a function of the concentration in Figure 3 for the two investigated ionic strengths.

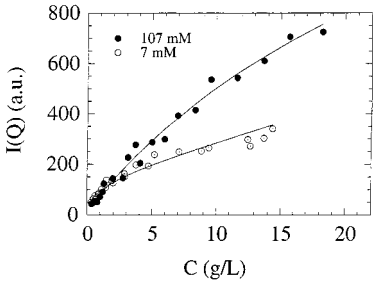

Figure 4. Intensity of the light scattered by β-LG at pH = 2.3 versus protein concentration, C, at $I_S = 7$ mM (open circles) and $I_S = 107$ mM (filled circles). The solid lines are best fits of the data according to the monomer−dimer equilibrium described in section 4.1.

The mutual diffusion coefficients show a steep and large increase for the lower ionic strength, while an initial small decrease, followed by a slow rise at higher concentrations, is observed for $I_S = 107$ mM. The different trend indicates a larger interaction between proteins at low ionic strength, as expected considering that the Debye screening length $1/\kappa_D$ (see eq 7) is changing from ≃30 Å at $I_S = 7$ mM to ≃10 Å at $I_S = 107$ mM. The extrapolation of the data taken at both the ionic strengths to the limit $C = 0$ gives very similar results, i.e. $D_0 = (9.2 \pm 0.1)\cdot 10^{-7}$ and $(9.4 \pm 0.1)\cdot 10^{-7}$ cm^2/s at $I_S = 7$ and 107 mM, respectively. From these coefficients, hydrodynamic radii of 23.2 ± 0.2 and 22.7 ± 0.2 Å were respectively calculated using the Stokes−Einstein relation

$$D_0 = \frac{k_B T}{6\pi\eta R_h} \tag{25}$$

with $\eta = 1.002$ cP.

The average light scattered intensities are reported as a function of protein concentration in Figure 4 for both the investigated ionic strengths. The 107 mM ionic strength data increase monotonically with C, while at lower ionic strength, intensities approach to a plateau and show values remarkably lower than those observed at higher ionic strength. The marked nonlinearity of the curve at $I_S = 7$ mM indicates the presence of relevant interparticle interactions. However, it is worth noting that, when extrapolating to $C = 0$, one finds similar slopes for both ionic strengths, suggesting that at infinite dilution the β-LG shows similar average molecular weight. Both the average scattered light intensities and the relaxation of its fluctuations are then consistent with enhanced protein−protein interactions at lower ionic strengths. Moreover, the initial decrease (see the inset of Figure 3) of the diffusion coefficient D versus concentration observed at $I_S = 107$ mM typically indicates the existence of a chemical equilibrium between two species; in the present case, we assume that monomers and dimers of β-LG are in the equilibrium described in eq 2.

We have fitted the diffusion coefficient and the average intensity data reported in Figures 3 and 4 to eqs 15 and 9, respectively. The model parameters are the charges of the monomer and dimer, Z_m and Z_d, their hydrodynamic radii, $R_{h,m}$ and $R_{h,d}$, the Hamacker constant, here kept at $5k_BT$, and the dissociation free energy, ΔG_{dis}, which is involved in the computation of the monomer fraction (see eq 2). In order to reduce the number of fitting parameters, the hydrodynamic radius of the dimer is assumed to scale with the mass ratio, $M_d/M_m = 2$ (i.e. $R_{h,d}/R_{h,m} = 2^{1/3}$) while the charge ratio Z_d/Z_m is fixed at 1.8, as discussed in section 3.1. A more accurate estimate of the ratio of the hydrodynamic radii, according to the hydrodynamic interactions between two touching beads,[49] is $R_{h,d}/R_{h,m} = 1.33$. On the other hand, when taking into account the ellipsoidal shape of the dimer by means of Perrin's equations,[50] the ratio of the radii must be corrected by a factor ≃0.96, which brings the estimate to $R_{h,d}/R_{h,m} \simeq 1.33 \times 0.96 = 1.277$. We have verified that the 1.3% understimation of the dimer hydrodynamic radius due to the use of the simpler law, $R_{h,d}/R_{h,m} = 2^{1/3}$, does not affect appreciably the results of the data analysis reported hereafter. A word of caution is necessary for the choice of the protein radius in the computation of the potentials (see eqs 12 and 13). As a matter of fact, the hydrodynamic radius estimated by extrapolating the diffusion coefficients to vanishing concentrations contains contributions from the protein−electrolytes interactions. Especially at low ionic strength, part of the electrolyte cloud around the protein suffers the same dragging force as the protein itself, inducing larger effective radii.[51,52] In a first but still accurate approximation,[51] from the extrapolated values of 23.2 ($I_S = 7$ mM) and 22.7 Å ($I_S = 107$ mM), "bare" monomer hydrodynamic radii $R^0_{h,m}$ of 19.1 ± 0.3 and 19.2 ± 0.4 Å, can be estimated, respectively. These values roughly correspond to the radius of the sphere with a volume equivalent to that of the monomer plus one hydration water shell. The average value $R^0_{h,m} = 19.15$ Å has been used to calculate the interaction potentials in the eqs 12 and 13.

Table 1. Results from the Fit of the Light Scattering and Photon Correlation Spectroscopy Data[a]

Photon Correlation Data

I_S (mM)	$D_{m,0}$ (10^{-7} cm^2/s)	Z_m	ΔG_{dis} (k_BT)	χ^2
7	9.2 ± 0.1	17 ± 2	4.4 ± 0.6	0.9
107	9.1 ± 0.2	16.5 ± 0.8	8.5 ± 0.9	1.4

Light Scattering Data

I_S (mM)	κ_{LS} (au)	B_{LS} (au)	Z_m	ΔG_{dis} (k_BT)	χ^2
7	85.5	35	19.5 ± 2	3.45 ± 1.1	2.5
107	30	34.4	16.8 ± 2	8.5 ± 0.7	8

[a] The reported errors are the standard deviations obtained by the fitting procedure.

In practice, the fitting parameters reduce to the monomer diffusion coefficient, $D_{m,0}$, and charge, Z_m, and to the dissociation free energy, ΔG_{dis}. The electrolyte screening is calculated via the Debye screening length using eq 7. The best fit curves are shown in Figure 3 and the fitting parameters are reported in Table 1. It can be observed that both high and low ionic strength data are well-reproduced by eq 15 over the whole investigated protein concentration range. Moreover, the dissociation free energy, ΔG_{dis}, is higher at 100 mM than at 7 mM. The initial decrease of the diffusion coefficient observed at $I_S = 107$ mM, when the protein concentration increases (see the inset in Figure 3), appears therefore mainly due to the association of monomers into dimers, i.e. follows the mass action law. At $C \geq 2M_mK_{dis}$ the mutual diffusion coefficient is affected *mainly* by the dimer−dimer interactions, which are weak due to the large electrostatic screening at this ionic strength. As a matter of fact, the protein charge is not remarkably different at the two ionic strengths, and the considerable difference in the interaction effects (i.e. the slope of D versus C) can be rationalized in terms of

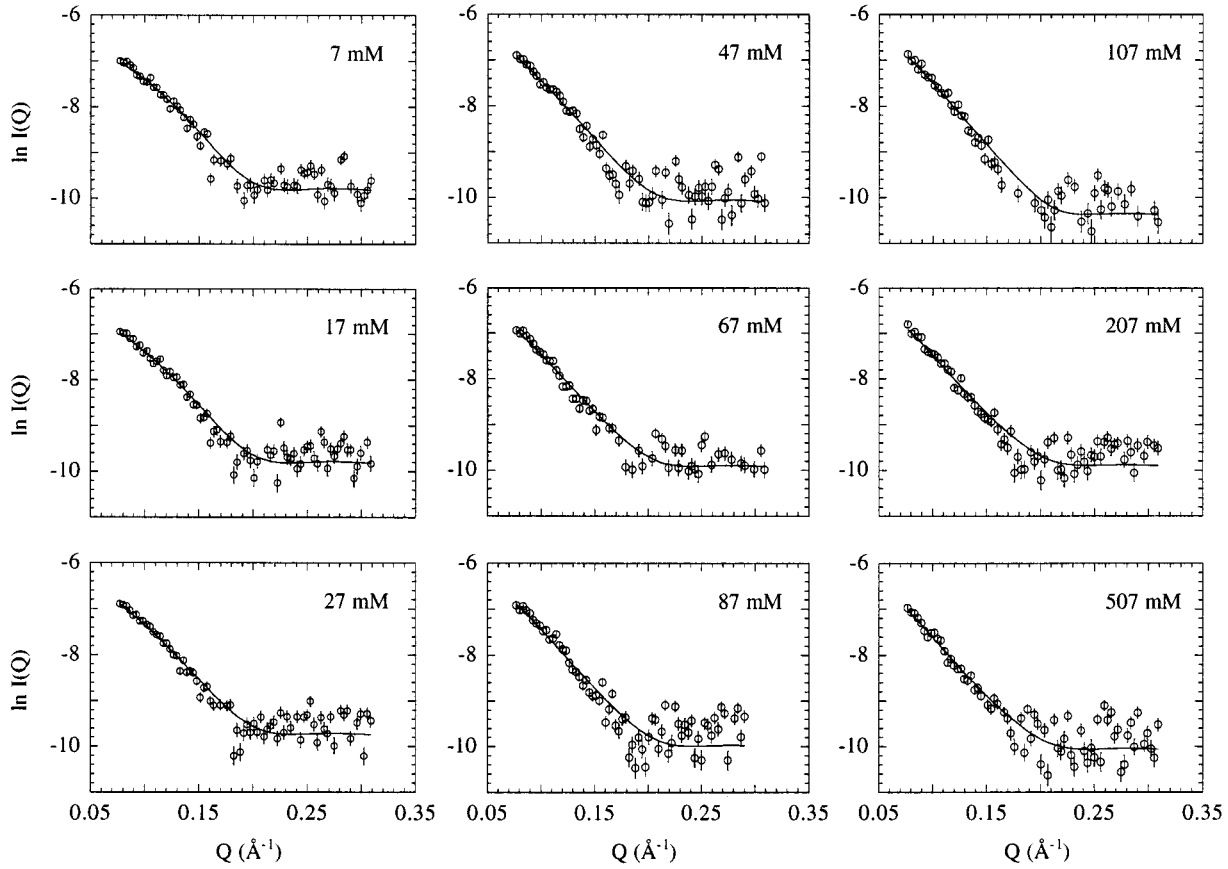

Figure 5. X-ray scattering data for β-LG at pH = 2.3 and concentration C = 10 g/L. The ionic strength of the solution is written in each frame. The continuous curves have been obtained by the global fitting procedure described in section 4.2.

Table 2. Results from the Fit of the SAXS Data[a]

I_S (mM)	$R_{g,a}$ (Å)	$I(0)$ (10^{-3} au)	κ_{XR} (10^{-7} au M^{-1})	B_{XR} (10^{-5} au)	$\bar{\chi}^2$
7	17.9 ± 0.3	1.82 ± 0.06	2.19 ± 0.02	4.85 ± 0.07	4.23
17	17.9 ± 0.4	1.84 ± 0.07	2.24 ± 0.01	4.87 ± 0.07	4.32
27	18.1 ± 0.3	2.01 ± 0.06	2.33 ± 0.02	5.30 ± 0.08	4.49
47	19.3 ± 0.4	2.04 ± 0.07	2.15 ± 0.02	3.66 ± 0.06	5.32
67	19.8 ± 0.3	2.24 ± 0.07	2.10 ± 0.01	4.45 ± 0.07	3.56
87	19.7 ± 0.4	2.25 ± 0.08	2.21 ± 0.01	4.07 ± 0.07	7.38
107	20.6 ± 0.4	2.34 ± 0.07	2.14 ± 0.01	2.66 ± 0.06	3.65
207	20.3 ± 0.4	2.31 ± 0.06	2.15 ± 0.01	4.57 ± 0.06	4.34
507	20.7 ± 0.3	2.16 ± 0.07	2.06 ± 0.01	3.89 ± 0.05	5.20

[a] The reported errors are the standard deviations obtained by the fitting procedures.

different electrostatic screening κ_D. In particular, the good agreement between the D_0 obtained from a simple extrapolation of diffusion coefficient data at I_S = 7 mM to zero concentration and the fitted monomer diffusion coefficients $D_{m,0}$ (see Table 1) should be also noticed: this is a direct verification that at a concentration of 0.2 g/L the equilibrium is greatly shifted to the monomeric form of β-LG.

We expect the interactions and the dissociation processes to be effective also on the trend of the average scattered intensity $I(Q)$ versus C (Figure 4). As shown in Figure 4, the experimental data are well-described by the function $I(Q)$, given by eqs 9 and 10, using the best fit parameters reported in Table 1. It can be noticed that the dissociation free energies and protein charges are in very good agreement with those found by diffusion coefficient analysis. This result confirms that the behavior observed is partially due to the association of monomers into dimers at increasing protein concentration.

4.2. Small-Angle X-ray Scattering. The results of SAXS measurements on solutions of β-LG at different ionic strengths are presented in Figure 5. At all the investigated ionic strengths, a preliminary Guinier analysis has been performed. In particular, it has been shown that for proteins the Guinier region can be extended up to $QR_{g,j} = 2$;[41] in the present case, the comparison of the Guinier law with the $P_j(Q)$ form factors of monomer and dimer confirmed the validity of this extention. Therefore, we applied the preliminary analysis up to $Q < 0.09$ Å^{-1}.

The intensities scattered at $Q = 0$ and the apparent radii of gyration, obtained using eq 21, are reported in Table 2. It can be observed that upon increasing the electrostatic screening, the gyration radius continuously increases from 18 to about 21 Å: these values correspond neither to the radius of gyration expected for the monomer ($R_{g,m}$ = 16.4 Å) nor to that of the dimer of β-LG ($R_{g,d}$ = 23.0 Å). Moreover, the scattering intensity at zero angle, $I(0)$, also increases as a function of the ionic strength. According to eqs 22 and 23, both the radius of gyration and the forward scattered intensity should increase when the protein monomer fraction, α, is decreasing. Therefore, the Guinier analysis suggests

the presence of a monomer−dimer equilibrium affected by the ionic strength of the solution.

The analysis of the distance distribution functions $p(r)$, calculated as indicated in section 2.2 from the experimental $I(Q)$, strongly confirms the presence of a monomer−dimer equilibrium. In Figure 2, the $p(r)$ functions are reported as a function of the ionic strength and are compared with the distance distribution functions calculated from the crystallographic data for the monomer and dimer of β-LG (see section 3.1). The comparison with the experimental curves is illustrative for the intermolecular association process. At low ionic strength, the experimental $p(r)$ functions are narrow and very similar to the one calculated for the monomer. The maximum particle dimension d_{max} can be estimated to be about 40 Å, which roughly corresponds to twice the radius of the monomeric protein. Data seem then to indicate that the monomers of β-LG are prevalent with respect to the dimeric form at low ionic strength. When the NaCl concentration increases, the $p(r)$ function continuously broadens and shifts toward larger dimensions, reflecting the expected increase in concentration of dimeric aggregates. At the largest ionic strength investigated, the maximum particle dimension, d_{max}, is about 60 Å, fairly close to the value observed for the β-LG dimeric structure (about 70 Å).

A more detailed analysis of the SAXS data has been then performed by fitting the scattered intensity with eq 18 and making use of the form factors $P_j(Q)$ calculated from the crystallographic structure of β-LG monomer and dimer, as described in section 3.1. However, in the fitting procedure, two relevant points have been considered: first, the monomer fraction α (that appears in eq 18) is directly related to the molecular dissociation free energy ΔG_{dis} (see eqs 1 and 2). Second, according to the approximate Debye−Hückel model described in the section 2, ΔG_{dis} is a function of the solution ionic strength I_S. Thus, it appears possible to simultaneoulsy fit all the scattering curves using just few physical parameters, all independent of I_S. In this way, by combining eq 18 with eqs 1, 2, and 4−7, a global fit of the SAXS data can directly give the molecular dissociation free energy ΔG_{dis} as a function of the solution ionic strength.

In particular, in eqs 6 and 7, the following parameters have been fixed: the monomer and dimer "bare" radii, $R^0_{h,m} = 19.15$ Å and $R^0_{h,d} = 24.13$ Å (as indicated in section 4.1); the counterion radius, $a = 1.5$ Å; the dielectric constant of the solvent, $\epsilon = 78.5$; the experimental temperature, $T = 293$ K; the ratio between the effective charges of dimer and monomer, $Z_d/Z_m = 1.8$ (see section 3.1). Therefore, in the global fitting procedure, the free parameters are only Z_m and ΔG_{nel}, the nonelectrostatic free energy. The merit functional to be minimized was defined as

$$\chi^2 = \frac{1}{N_S}\sum_{k=1}^{N_S}\bar{\chi}_k^{\,2}$$

$$\bar{\chi}_k^{\,2} = \frac{1}{N_{Q,k}}\sum_{l=1}^{N_{Q,k}}\left[\frac{I_k^{exp}(Q_l) - I_k^{mod}(Q_l)}{\sigma_l}\right]^2 \qquad (26)$$

where N_S is the number of scattering curves under analysis, $N_{Q,k}$ is the number of experimental points in the kth SAXS curve, and σ_l is the experimental uncertainty of the intensity $I_k^{exp}(Q_l)$ of the lth point. $I_k^{mod}(Q_l)$ is the corresponding intensity calculated from eq 18; for each experiment, the calibration factor κ_{XR} and the flat background B_{XR} have been adjusted from a linear least squares fit of $I_k^{exp}(Q)$.

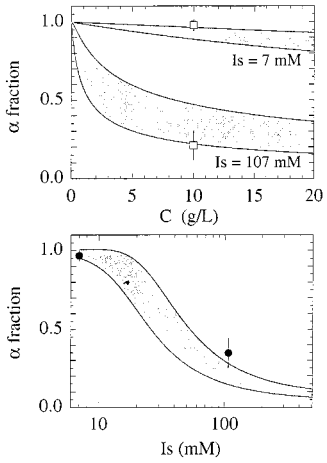

Figure 6. β-LG monomer α fraction at pH = 2.3. Upper frame: dependence on the protein concentration C. The bands show the α range values obtained from the analysis of the diffusion coefficient data at 7 and 107 mM of ionic strengths as described in section 4.1. For comparison, the corresponding values obtained from SAXS data are reported as open squares. Lower frame: dependence on the ionic strength I_S of the solution at $C = 10$ g/L. The band shows the α range values obtained from the global fit procedure of SAXS data as described in section 4.2; filled circles refer to α values obtained by fitting the diffusion coefficient data.

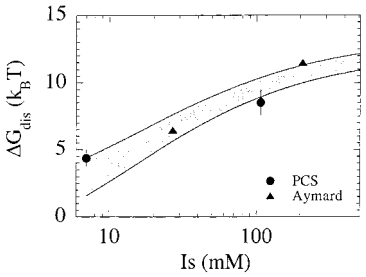

Figure 7. Dissociation free energy, ΔG_{dis}, as a function of the ionic strength of the solution. The band shows the ΔG_{dis} range values obtained by the global fitting procedure of the SAXS data as described in section 4.2. Filled circles refer to the ΔG_{dis} obtained by fitting the diffusion coefficient data. Filled triangles refer to dissociation free energy values as reported by Aymard et al.[8]

The best fit global parameters, which correspond to the fitting curves shown in Figure 5, were $Z_m = 16 \pm 1$ and $\Delta G_{nel}/k_BT = 13.1 \pm 0.6$, which produce a merit functional $\chi^2 = 0.92$. In Table 2 the κ_{XR}, B_{XR}, and $\bar{\chi}^2$ values obtained for each experiment are reported. Noticeable is the fact that the calibration factors κ_{XR}, which only depend on the experimental set-up and then are expected to be equal, are rather similar, indicating the goodness of the proposed model (including the assumption that the structure factor $S(Q)$ is unity). Moreover, the flat backgrounds are significatively small, validating the assumption $B_{XR} = 0$ in the Guinier analysis previously discussed.

As a final result of the global fit procedure, in Figures 6 (lower panel) and 7 the monomer fraction α and the corresponding ΔG_{dis} are shown as a function of the solution ionic strength I_S.

4.3. Discussion. The structural properties of β-lactoglobulin in acidic solution (pH = 2.3) have been

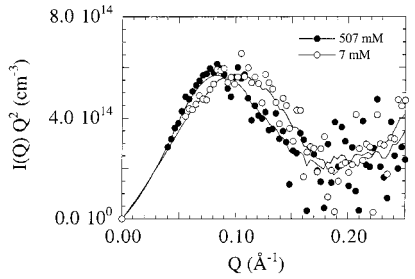

Figure 8. Kratky plots of SAXS curves from β-LG at pH = 2.3 and C = 10 g/L obtained at ionic strengths of 7 (open circles) and 507 (filled circles) mM. The solid lines are the results of smooth fitting of the experimental data.

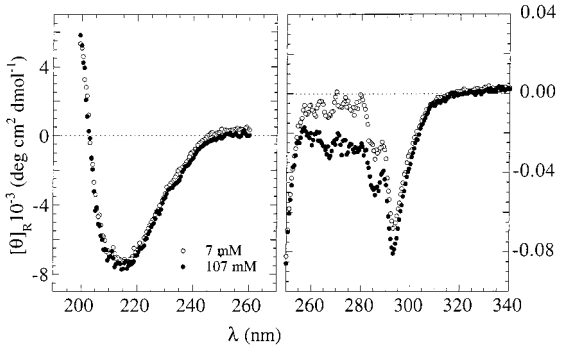

Figure 9. Circular dichroism spectra in the far-UV (left frame) and near-UV (right frame) of β-LG at pH = 2.3 and C = 10 g/L at ionic strengths of 7 (open circles) and 107 (filled circles) mM.

studied by light and X-ray scattering over a wide range of ionic strengths and concentrations; a coherent picture emerges from both measurements. The experimental results are in fact consistent with the existence of a monomer−dimer equilibrium, strongly sensitive to the concentration of added electrolytes.

However, in order to draw more quantitative conclusions, one should also account for subtle effects such as partial protein unfolding and/or electrolyte−protein interactions which could affect the structural and dynamic properties of the β-LG in solution. As to the radius of gyration and SAXS analysis, the observed changes with ionic strength cannot be ascribed to an extensive denaturation process eventually occurring at acidic pH. As a matter of fact, the Kratky plots of the SAXS profiles (two of them are reported as examples in Figure 8) show a peak at all the ionic strengths analyzed, confirming the presence of a compact globular structure in all the investigated conditions. Moreover, also circular dichroism measurements, performed at I_S = 7 and 107 mM in the near-UV region and shown in Figure 9, indicate that the secondary structure of the protein is well-preserved under these experimental conditions. According to previous works,[53,54] it should be noticed that the small changes in the ellipticity detected in the near-UV region between low and high ionic strengths may be ascribed to small changes in residue mobilities. As a matter of fact, β-LG is thought to be, at acidic pH, in a molten globule state corresponding to a combination of a more open conformation and a compact core.[10] As to the other parameter characterizing the molecular size, i.e., the hydrodynamic radius of the monomer, one estimates $R^0_{h,m}$ = 19.1 ± 0.3 and 19.2 ± 0.4 Å at I_S = 7 and 107 mM, respectively. The good agreement confirms that the molecular volume is not appreciably changed upon raising the ionic strength. However, minor secondary structure variations cannot be excluded at low ionic strengths. Partial opening of external loops could be involved in the observed small changes in CD spectra and would imply a small increase in the hydrodynamic radius, which are within the experimental uncertainties of the PCS measurements.

Since the side effects considered above seem to affect only slightly the changes observed in the structural and dynamic parameters of the β-LG in solution, one can now draw more quantitative conclusions about the association behavior of β-LG as a function of ionic strength. At first, it is rewarding that techniques with very different resolutions give a coherent picture of the monomer−dimer equilibrium of β-LG in acidic conditions. The global fit procedure used to analyze SAXS data gives a continuous variation of the monomer fraction α and of the molecular dissociation free energy ΔG_{dis} as a function of solution ionic strength I_S (Figures 6 and 7). An analogous estimate can be made from the PCS results: by inverting eqs 1 and 2 and using the values of ΔG_{dis} reported in Table 1, one can evaluate the monomer fraction α at I_S = 7 and 107 mM. The corresponding values are reported in Figure 6 (upper panel) as a function of the protein concentration for each of the two analyzed ionic strengths. In the same panel, open squares indicate the data obtained by SAXS measurements; the agreement is excellent. On the other hand, the α values obtained at C = 10 g/L by means of PCS measurements are reported as filled circles in the plot versus the ionic strength shown in the lower panel of Figure 6. Again noticeable is the good agreement between the SAXS and the PCS data, though the PCS analysis slightly overestimates (underestimates) the monomer fraction compared to the X-ray scattering results at I_S = 107 mM (I_S = 7 mM).

The plot of ΔG_{dis} versus the ionic strength shown in Figure 7 indicates a variation of about $7k_BT$ when passing from I_S = 7 mM to I_S = 507 mM, a result substantially confirmed by PCS data (see the filled circles in Figure 7) and in very good agreement with previous data from Aymard et al.[8] This observed small change in ΔG_{dis} may be somehow surprising when considering that the Debye screening length $1/\kappa_D$ changes from 30 to about 4 Å and that the protein carries 20 basic amino acids per monomer, which at pH = 2.3 would correspond to a maximum of 20 proton charges on the protein surface. That the observed change in ΔG_{dis} can be described by the Debye−Hückel theory is not surprising, even though the surface potentials at I_S = 7 mM is as high as ≃3.5 k_BT/q (q is the proton charge). As recently shown by Fogolari et al.,[55] two opposite contributions to the electrostatic ΔG partially compensate to reduce the discrepancy between the estimates of the ΔG made through the linearized and nonlinear Poisson−Boltzmann equations. The Debye−Hückel model is then expected to give a reasonable account for the dissociation free energy[28] in the range of ionic strengths explored here.

More interestingly, the Debye−Hückel model for the β-LG dissociation appears incompatible with a dimer−monomer charge ratio Z_d/Z_m = 2. As a matter of fact, the experimental X-ray data can be reasonably well-reproduced also using in the global fitting procedure charge ratios $1.75 < Z_d/Z_m < 2$, finding however large variations for the effective monomer charge (see Figure 10). In particular, it can be observed that the dimer charge cannot be larger than $2Z_m$, while below Z_d/Z_m =

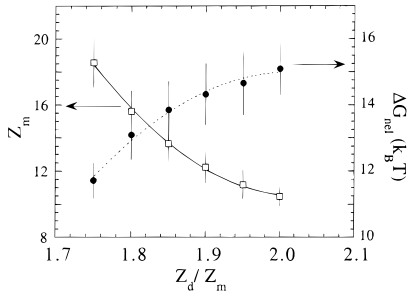

Figure 10. Monomer charge, Z_m, and nonelectrostatic dissociation free energy, ΔG_{nel}, obtained by the global fitting procedure of the SAXS data using different dimer−monomer charge ratios Z_d/Z_m. See detail in section 4.2. Lines are a guide to the eyes.

1.75, the monomer charge assumes values larger than 20, devoid of physical sense. From the figure, it appears that the monomer charge $Z_m \simeq 17$, which results from PCS data analysis (see Table 1), is obtained when $Z_d/Z_m \simeq 1.8$, as expected if two basic amino acids per monomer would not contribute to the total dimer effective charge. This result is fully consistent with the structural feature of the dimer discussed in the section 3.1 (see also Figure 1).

5. Conclusion

The dimerization equilibrium of β-LG has been studied by SAXS and PCS, two scattering techniques employing electromagnetic radiation with wavelength separated by 4 orders of magnitude. It is rewarding that both the experimental results can be consistently analyzed in terms of a β-LG dimerization process enhanced by the ionic strength of the solution. The analysis of the diffusion coefficient and the average scattered light versus the protein concentration yields estimates of the protein effective charge and of the monomer fraction. In addition to this, a global fit procedure to analyze SAXS data from β-LG solutions in the frame of a simple Debye−Hückel model for charged spheres gives the dissociation free energy in a wide range of ionic strength. We have also shown that the corresponding increase of about $7k_BT$ in the dissociation free energy with the ionic strength is in good agreement with the prediction of a simple model based on the linearized Poisson−Boltzmann theory and that the experimental data are fully compatible with the β-LG structure when assuming that two charges per monomer are hidden after dimerization.

Acknowledgment. This work has been partially supported by the grant for the Advanced Research Project on Protein Crystallization "Procry" of the National Institute for the Physics of Matter.

References and Notes

(1) Joss, L. A.; Ralston, G. B. *Analytical Biochem.* **1996**, *236* (1), 20−26.
(2) Casal, H. L.; Kohler, U.; Mantsch, H. N. *Biochim. Biophys. Acta* **1988**, *957*, 11−20.
(3) Dong, A. C.; Prestrelski, S. J.; Carpenter, S. D.; Allison, J. F. *J. Pharm. Sci.* **1995**, *84* (4), 415−424.
(4) Renard, D.; Lefebvre, J.; Griffin, M. C. A.; Griffin, W. G. *Int. J. Biol. Macromol.* **1998**, *22* (1), 41−49.
(5) Wahl, P.; Timasheff, S. N. *Biochemistry* **1969**, *8* (7), 2945−2949.
(6) Witz, J.; Timasheff, S. N.; Luzzati, V. *J. Am. Chem. Soc.* **1963**, *86*, 168−173.
(7) Arai, M.; Ikura, T.; Semisotnov, G. V.; Kihara, H.; Amemiya, Y.; Kuwajima, K. *J. Mol. Biol.* **1998**, *275*, 149−162.
(8) Aymard, P.; Durand, D.; Nicolai, T. *Int. J. Biol. Macromol.* **1996**, *19*, 213−221.
(9) Elofsson, U. M.; Paulsson, M. A.; Sellers, P.; Arnebrant, T. *J. Colloid Interface Sci.* **1996**, *183* (2), 408−415.
(10) Molinari, H.; Ragona, L.; Varani, L.; Musco, G.; Consonni, R.; Zetta, L.; Monaco, H. *FEBS Lett.* **1996**, *381*, 237−243.
(11) Brownlow, S.; Cabral, J. H. M.; Cooper, R.; Flower, D. R.; Yewdall, S. J.; Polikarpov, I.; North, A. C. T.; Sawyer, L. *Structure* **1997**, *5*, 481−495.
(12) Ikeguchi, M.; Kato, S.; Shimizu, A.; Sugai, S. *Proteins* **1997**, *27* (4), 567−575.
(13) Subramaniam, V.; Steel, D. G.; Gafni, A. *Protein Sci.* **1996**, *5* (10), 2089−2094.
(14) Verheul, M.; Pedersen, J. S.; Roefs, S. P. F. M.; de Kruif, K. J. *Biopolymers* **1999**, *49*, 11−20.
(15) Valente-Mesquita, V. L.; Botelho, M. M.; Ferreira, S. T. *Biophys. J.* **1998**, *75*, 471−476.
(16) Dufour, E.; Roger, P.; Haertle, T. *J. Protein Chem.* **1992**, *11* (6), 645−652.
(17) Dufour, E.; Genot, C.; Haertle, T. *Biochim. Biophys. Acta* **1994**, *1205* (1), 105−112.
(18) Cairoli, S.; Iametti, S.; Bonomi, F. *J. Protein Chem.* **1994**, *13* (3), 347−354.
(19) Uversky, V. N.; Narizhneva, N. V.; Kirschstein, S. O.; Winter, S.; Lober, G. *Folding Design* **1997**, *2* (3), 163−172.
(20) Schmitz, K. S. In *An introduction to dynamic light scattering by macromolecules*; Academic: Boston, 1990.
(21) Pecora, R. In *Dynamic light scattering. Applications of photon correlation spectroscopy*; Pecora, R., Ed.; Plenum: New York, 1985.
(22) Beretta, S.; Chirico, G.; Lunelli, L.; Baldini, G. *Appl. Optics* **1996**, *35*, 3763−3770.
(23) Beretta, S.; Chirico, G.; Arosio, D.; Baldini, G. *J. Chem. Phys.* **1997**, *106*, 8427−8435.
(24) Glatter, O.; Kratky, O. In *Small-Angle X-ray Scattering*; Academic: New York, 1982.
(25) Jacrot, B. *Rep. Prog. Phys.* **1976**, *39*, 911−953.
(26) Chirico, G.; Baldini, G. *J. Chem. Phys.* **1996**, *104*, 6009−6019.
(27) Guinier, A.; Fournet, G. In *Small angle scattering of X-ray*; Wiley: New York, 1955.
(28) Tanford, C. In *Physical Chemistry of Macromolecules*; Wiley: New York, 1961.
(29) Schmitz, K. S. In *Macroions in solution and colloidal suspension*; VCH: New York, 1993.
(30) Hansen, J. P.; Hayter, J. B. *Mol. Phys.* **1982**, *46*, 651−656.
(31) Corti, M.; Degiorgio, V. *J. Phys. Chem.* **1981**, *85*, 711−717.
(32) Kuehner, D. E.; Heyer, C.; Rämsch, C.; Fornefeld, U. M.; Blanch, H. W.; Prausnitz, J. M. *Biophys. J.* **1997**, *73*, 3211−3224.
(33) Dhont, J. K. G. In *An Introduction to Dynamics of Colloids*; Elsevier: Amsterdam, 1996.
(34) Ohshima, H.; Mishonova, E.; Alexov, E. *Biophys. Chem.* **1996**, *57*, 189−203.
(35) Muschol, M.; Rosenberger, F. *J. Chem. Phys.* **1995**, *103*, 10424−10432.
(36) Felderhof, B. U. J. *J. Phys. A: Math. Gen.* **1978**, *11*, 929−937.
(37) Phillies, G. D. J. *J. Phys. Chem.* **1995**, *99*, 4265−4272.
(38) Batchelor, J. K. *J. Fluid. Mech.* **1976**, *74*, 1−29.
(39) Ashcroft, N. W.; Lekner, J. *Phys. Rev.* **1966**, *145*, 83−90.
(40) Spinozzi, F.; Carsughi, F.; Mariani, P. *J. Chem. Phys.* **1998**, *109*, 10148−10158.
(41) Kataoka, M.; Nishii, I.; Fujisawa, T.; Ueki, T.; Tokunaga, F.; Goto, Y. *J. Mol. Biol.* **1995**, *249*, 215−228.
(42) Kataoka, M.; Hagihara, Y.; Mihara, K.; Goto, Y. *J. Mol. Biol.* **1993**, *229*, 591−596.
(43) Semisotnov, G. V.; Kihara, H.; Kotova, N. V.; Kimura, K.; Amemiya, Y.; Wakabayashi, K.; Serdyuk, I. N.; Timchenko, A. A.; Chiba, K.; Nikaido, K.; Ikura, T.; Kuwajima, K. *J. Mol. Biol.* **1996**, *262*, 559−574.
(44) Jacrot, B.; Zaccai, G. *Biopolymers* **1981**, *20*, 2413−2426.
(45) Protein Data Bank, www.pdb.bnl.gov, entry 1BEB.
(46) Mariani, P.; Carsughi, F.; Spinozzi, F.; Romanzetti, S.; Meier, G.; Casadio, R.; Bergamini, C. M. Submitted.
(47) Svergun, D. I. *J. Appl. Crystallogr.* **1997**, *30*, 792−797.
(48) Chirico, G.; Gardella, M. *Appl. Optics* **1999**, *38*, 2059−2067.
(49) Ermak, D. L.; McCammon, J. A. *J. Chem. Phys.* **1978**, *69*, 1352−1359.
(50) Dubin, S. B.; Clark, N. A.; Benedek, G. B. *J. Chem. Phys.* **1973**, *54*, 5158−66.
(51) Schurr, J. M. *Chem. Phys.* **1980**, *45*, 119−132.

(52) Hernandez-Contreras, M.; Alarcón-Waess, O.; Medina-Noyola, M. *J. Chem. Phys.* **1997**, *106*, 2492−2501.
(53) Ptitsyn, O. B. *Curr. Opin. Struct. Biol.* **1995**, *5*, 174−178.
(54) Mizuguchi, M.; Arai, M.; Ke, Y.; Nitta, K.; Kuwajima, K. *J. Mol. Biol.* **1998**, *283*, 1265−1277.
(55) Fogolari, F.; Zuccato, P.; Esposito, G.; Viglino, P. *Biophys. J.* **1999**, *76*, 1−16.

MA990709U